Lack of resolvable titanium stable isotopic variations in bulk chondrites

Deng, Zhengbin; Moynier, Frédéric; van Zuilen, Kirsten; Sossi, Paolo A.; Pringle, Emily A.; Chaussidon, Marc

published in
Geochimica et Cosmochimica Acta
2018

DOI (link to publisher)
10.1016/j.gca.2018.06.016

document version
Publisher's PDF, also known as Version of record

Available online at www.sciencedirect.com

ScienceDirect

Geochimica et Cosmochimica Acta 239 (2018) 409–419

Geochimica et Cosmochimica Acta

www.elsevier.com/locate/gca

Lack of resolvable titanium stable isotopic variations in bulk chondrites

Zhengbin Deng [a,*], Frédéric Moynier [a,b], Kirsten van Zuilen [a,1], Paolo A. Sossi [a], Emily A. Pringle [a], Marc Chaussidon [a]

[a] Institut de Physique du Globe de Paris, Université Paris Diderot, Université Sorbonne Paris Cité, CNRS UMR 7154, 1 rue Jussieu, 75005 Paris, France

[b] Institut Universitaire de France, Paris, France

Received 13 November 2017; accepted in revised form 15 June 2018; available online 23 June 2018

Abstract

Titanium and calcium are both refractory lithophile elements. Significant stable isotopic variations on Ti and Ca have been documented within calcium, aluminum-rich inclusions (CAIs) in carbonaceous chondrites. To trace the condensation history of Ti in the solar nebula, we conducted a high-precision double-spike Ti stable isotopic study on a large set of chondrites. The studied chondrites have a homogeneous bulk Ti stable isotopic composition ($\delta^{49/47}Ti_{IPGP\text{-}Ti} = -0.069 \pm 0.018‰$, 2se, n = 22, i.e., the per mil deviation of the $^{49}Ti/^{47}Ti$ ratios relative to the IPGP-Ti reference material). The homogeneity across eleven chondrite groups implies that chondrites have acquired, through the condensation sequence at equilibrium, the average stable isotopic composition of Ti in the refractory solids that condensed early in the solar nebula. In contrast, the light Ca stable isotopic compositions of bulk chondrites can be attributed to either the presence of CAIs (CV-, CM- and CO-type) or parent-body aqueous alteration (CR- and CI-type).

Keywords: Titanium isotopes; Calcium isotopes; Chondrites; Double spike

1. INTRODUCTION

Chondrites are undifferentiated meteorites with chemical compositions (except H, He, Li, C, N, O and noble gases) close to those of the solar photosphere (in particular CI-type chondrites; Anders and Grevesse, 1989). Since the discovery of oxygen isotopic anomalies in carbonaceous chondrites (Clayton et al., 1973), mass-independent isotopic variations of various elements such as Ca (e.g., Jungck et al., 1984; Niederer and Papanastassiou, 1984; Simon et al., 2009; Schiller et al., 2015; Huang and Jacobsen, 2017), Ti (e.g., Niemeyer and Lugmair, 1981, 1984; Niederer et al., 1985; Trinquier et al., 2009), Cr (e.g., Trinquier et al., 2008; Birck and Allègre, 1985; Papanastassiou, 1986), Ni (e.g., Steele et al., 2012) or V (Sossi et al., 2017) have been used to trace the heterogeneity of the solar proto-planetary disk, the effect of early solar irradiation or to identify the materials that accreted to form the terrestrial planets (see the recent reviews in Teng et al. (2017) for other elements such as Fe, Mg, Zn, Mo, etc.). In contrast, mass-dependent isotopic variations in planetary reservoirs can be used to study a number of processes, such as nebular condensation and evaporation (e.g., Niederer and Papanastassiou, 1984; Niederer et al., 1985; Simon and DePaolo, 2010), electromagnetic separation in the solar nebula (e.g., Moynier et al., 2006, 2015), syn- or post-accretion processes including metal-silicate

* Corresponding author.
E-mail address: deng@ipgp.fr (Z. Deng).
[1] Department of Earth Sciences, Vrije Universiteit Amsterdam, Amsterdam, The Netherlands

https://doi.org/10.1016/j.gca.2018.06.016
0016-7037/

differentiation (e.g., Shahar et al., 2011), volatile depletion (e.g., Paniello et al., 2012; Pringle et al. 2014; Day and Moynier 2014; Hin et al., 2017), magmatic differentiation (e.g., Teng et al., 2010; Sossi and O'Neill, 2017; Greber et al., 2017b) and parent-body aqueous alteration (Clayton and Mayeda, 1999). Among these, evaporation and condensation driven by thermal events in the solar nebula are fundamental to shape the isotopic composition of early solar system materials (e.g., Niederer and Papanastassiou, 1984; Niederer et al., 1985; Simon and DePaolo, 2010; Davis et al., 1990; Luck et al. 2005; Kato and Moynier 2017; Pringle and Moynier, 2017; Hin et al., 2017). As shown by the Ca isotopic studies of aluminum-rich inclusions (CAIs) and experimental samples, the magnitude of isotopic fractionation resulting from evaporation and condensation in vacuum is proportional to the square root of the ratio of the masses of the two isotopes (Richter et al., 2002). This approximation holds for Ca and Ti, for which the relative mass difference, and hence isotope fractionation, is larger for Ca (g) relative to TiO_2 (g) at 2000 °C (Zhang et al., 2014). Nevertheless, evaporation at lower temperatures of elements such as Si, Mg and K is subject to a smaller isotopic fractionation than predicted under vacuum, potentially due to diffusion in the gas phase (Davis et al., 1990; Richter et al., 2011; Mendybaev et al., 2013).

In the solar nebula, Ti and Ca are both refractory lithophile elements (50% T_C of 1582 K for Ti and 1517 K for Ca; Lodders et al., 2003), limiting the potential for modification of their isotope signatures by evaporation/condensation. Nonetheless, it was shown that CAIs exhibited large mass-dependent isotopic variations of Ca, Ti, Mg and O, but there was no correlation between the mass-dependent isotopic variations of Ti and those of Ca (Niederer and Papanastassiou, 1984; Niederer et al., 1985). Recently, Simon et al. (2017) and Davis et al. (2018) confirmed the different stable isotopic behaviors of Ti and Ca in CAIs: Ca tends to be enriched in the lighter isotopes while Ti can be both isotopically heavy or light. In contrast to the isotopic variations observed in CAIs by Simon et al. (2017), 3‰/amu for Ca and 0.7‰/amu for Ti, and by Niederer et al. (1985), 2.6‰/amu for Ca and 1.2‰/amu for Ti, the magnitude of isotopic fractionation is larger for Ca (5‰/amu) and Ti (4‰/amu) in the CAI samples from Davis et al. (2018).

The distinction in the mass-dependent isotope fractionation of Ti and Ca is borne out in the composition of carbonaceous chondrites at the bulk scale. Individual carbonaceous chondrite groups are characterized by a progressive enrichment in the lighter Ca isotopes in the order $CO < CM \leq CI \leq CR \leq CV$ (Simon and DePaolo, 2010; Valdes et al., 2014; Amsellem et al., 2017; Huang and Jacobsen, 2017). The CR- and CV-type chondrites are up to 0.25‰/amu lighter in Ca than the bulk silicate Earth (BSE; Huang et al., 2010; Kang et al., 2017). Titanium isotopic studies of bulk chondrites are very limited with only two studies reporting a total of 6 data for carbonaceous chondrites. Williams (2015) found that both Murchison and Allende chondrites were isotopically heavier than terrestrial basalts, whereas Greber et al. (2017a) reported no resolvable Ti stable isotopic variations within a precision of ±0.02‰/amu for Lancé (CO), Murray (CM), Orgueil (CI) and Allende (CV), which are similar to terrestrial basalts. Greber et al. (2017a) inferred that the Ca stable isotopic variations in bulk chondrites could be explained by the varying abundances of CAIs. While this conclusion may work for chondrite samples showing high contents of CAIs (e.g., the CV- and CM-type), it cannot explain the ~0.1–0.2‰/amu isotopically lighter Ca in CI- and CR-type chondrites compared to CO-type, ordinary and enstatite chondrites (Valdes et al., 2014) because these groups are CAI-poor (≈ 0%; Hezel and Palme, 2008). The origin of Ca stable isotopic variations in bulk carbonaceous chondrites is puzzling since, among the most abundant elements (e.g., oxygen, magnesium, silicon, calcium and iron) oxygen is the only other element that shows significant mass-dependent isotopic variation among meteorite classes (Clayton et al., 1988; Teng et al., 2010; Sossi et al., 2016).

To understand the stable isotopic behaviors of Ti in chondritic materials, a large set of chondrite samples were analyzed for their Ti isotopic compositions by a ^{47}Ti-^{49}Ti double spike technique. The new Ti isotopic data allow us to evaluate the processes that may have induced Ti variations in chondrites, and further trace the condensation history of Ti in the solar nebula.

2. SAMPLES AND ANALYTICAL METHODS

2.1. Samples

Terrestrial samples. Four international geological reference materials from the U.S. Geological Survey, including a Hawaiian basalt (BHVO-2), an Icelandic basalt (BIR-1), a Columbia River basalt (BCR-2) and a Guano Valley andesite (AGV-1), were analyzed. The OL-Ti standard used in Millet and Dauphas (2014) and Greber et al. (2017a) was calibrated relative to the IPGP-Ti standard (Table 1).

Chondrites. Chondrites studied here include one CI-chondrite (Orgueil, CI1), two CM (Murchison, CM2; Cold Bokkeveld, CM2), three CO (Ornans, CO3.4; Lancé, CO3.5; and Isna, CO3.8), two CV (Allende, CV3; and Vigarano, CV3), one CK (Karoonda, CK4), two CR (RBT04133, CR2; A881595, CR2), one CH (PCA91467, CH3), four L (Hallingeberg, L3.4; Saratov, L4; Tedjera, L5; and l'Aigle, L6), two LL (Olivenza, LL5; and Cherokee Springs, LL6), one EL (Khairpur, EL6) and three EH (Sahara 97096, EH3; GRO95517, EH3; and Indarch, EH4) chondrites (Table 2).

2.2. Methods

2.2.1. Sample digestion

Three different methods for sample digestion were tested, for all of them, meteorite pieces of ~1 g were crushed into fine-grained powders (200–300 mesh, i.e., with grain size ≤ 75 μm) using an agate mortar and pestle.

HF-HNO_3 hot-plate digestion. About 6–20 mg of sample powder containing 5–22 μg Ti were weighed into 7 ml Savillex PFA beakers, and 2 ml 26 M HF and 1 ml 16 M HNO_3 were added and left overnight at room temperature before

Table 1
Titanium stable isotopic compositions of reference materials in this study and literature.

Sample	Lithology/Type	$\delta^{49/47}Ti_{IPGP\text{-}Ti}$ (‰)	2se	n
OL-Ti_Spray chamber	Ti-standard	−0.158	0.008	8
OL-Ti_Apex		−0.140	0.011	8
BHVO-2_this study	basalt	−0.129	0.011	18
BHVO-2_W2015		−0.139	0.024	6
BHVO-2_M2014+2016		−0.119	0.014	12
AGV-1_this study	andesite	−0.060	0.012	4
AGV-2_W2015		−0.078	0.052	5
AGV-1_M2014+2016		−0.056	0.031	2
BIR-1-this study	basalt	−0.188	0.010	27
BIR-1_M2014+2016		−0.206	0.024	3
BCR-2_this study	basalt	−0.148	0.010	8
BCR-2_W2015		−0.127	0.026	6
BCR-2_M2014+2016		−0.155	0.012	12

Note: "W2015" stands for the reference Williams (2015), and "M2014+2016" represents the references Millet and Dauphas (2014) and Millet et al. (2016). The reported $\delta^{49/47}Ti_{IPGP\text{-}Ti}$ values here have included a correction of $+0.022 \pm 0.009$‰ with error propagation to account for the Ca effects from the used double spike. The data can be rescaled onto the OL-Ti standard using $\delta^{49/47}Ti_{IPGP\text{-}Ti} = -0.140 \pm 0.011$‰ for OL-Ti.

Table 2
Titanium stable isotopic compositions of chondrite samples in this study.

Sample	Lithology/type	$\delta^{49/47}Ti_{IPGP\text{-}Ti}$ (‰)	2se	n
Orgueil	CI1	−0.063	0.041	4
Murchison	CM2	−0.103	0.016	7
Cold Bokkeveld	CM2	−0.112	0.015	3
Ornans	CO3.4	−0.061	0.029	6
Lance	CO3.5	−0.060	0.016	9
Isna	CO3.8	−0.030	0.028	9
Allende	CV3	−0.028	0.028	10
Vigarano	CV3	+0.014	0.024	5
Karoonda	CK4	−0.072	0.009	2
RBT04133	CR2	−0.026	0.009	2
A881595	CR2	−0.079	0.025	6
PCA91467	CH3	−0.075	0.029	2
Hallingeberg.	L3.4	−0.041	0.022	4
Saratov	L4	−0.074	0.011	2
Tadjera	L5	−0.051	0.010	4
l'Aigle	L6	−0.054	0.012	7
Olivenza	LL5	−0.145	0.018	3
Cherokee Springs	LL6	−0.023	0.015	2
Khairpur	EL6	−0.054	0.043	2
Sahara 97096	EH3	−0.124	0.016	7
GRO95517	EH3	−0.162	0.011	3
Indarch	EH4	−0.096	0.020	5
Average		***−0.069***	***0.018***	***22***

Note: More details have been provided in Supplementary Table S6. The data can be rescaled onto the OL-Ti standard by using $\delta^{49/47}Ti_{IPGP\text{-}Ti} = -0.140 \pm 0.011$‰ for OL-Ti.

being evaporated to dryness at ~100 °C. Subsequently, 2 ml 26 M HF and 1 ml 16 M HNO_3 were added and the closed beakers were placed on a hot plate at ~100 °C for three days. After evaporation to dryness, the sample residues were dissolved in 3 ml 6 M HCl at ~130 °C for three days to decompose the fluorides that formed during HF digestion.

Parr bomb digestion. Sample powders of 8–25 mg containing 7–21 μg were weighed into 23 ml PTFE beakers. Subsequently, 2 ml 26 M HF and 1 ml 16 M HNO_3 were added before placing the PTFE beakers into stainless-steel digestion vessels (Parr bombs). High-pressure digestion was achieved by heating the sealed vessels within a ventilation oven at 140 °C for two days. Afterwards, the PTFE beakers were taken out and the samples evaporated to dryness, before being dissolved in 3 ml 6 M HCl in the ventilation oven at 140 °C for two days for fluoride decomposition.

Alkali Fusion. Solutions of the digested chondrites including samples of Orgueil, Murchison, Ornans, Lancé, Allende, Vigarano, A881595, Hallingeberg, Saratov, Tadjena, l'Aigle, Olivenza and Cherokee Springs, were the same as used in Pringle et al. (2013). Another set of chondrite samples, including samples of Murchison, Cold Bokkeveld, Allende, Lancé, Isna, Vigarano, l'Aigle, Sahara 97096, GRO95517 and Indarch, were freshly dissolved at IPGP following the alkali fusion protocol of Pringle et al. (2013) (Table 2). For all the samples, about 7–15 mg of sample powder were weighed into Ag crucibles with addition of ~200 mg NaOH pellets (99.99% trace metal basis, Sigma Aldrich Company). Fusion was conducted in a furnace in air at ~720 °C for 15 min. The fused samples were finally dissolved in about 1 M HNO_3 at room temperature.

2.2.2. Chromatographic Ti purification

Before chromatographic purification, an adequate amount of ^{47}Ti-^{49}Ti double spike (see below) was added to an aliquot of each dissolved sample after the Ti concentration was determined by a Agilent 7900 Series Inductively-Coupled-Plasma Mass-Spectrometer (ICP-MS)

at IPGP. Since high-precision mass-independent Ti isotopic compositions of bulk chondrites have been well documented in Trinquier et al. (2009) and Zhang et al. (2012), only spiked aliquots were processed in this study. The spiked solutions were placed in closed beakers on a hot plate at about 100 °C for at least one hour, to ensure sufficient equilibration between sample and double spike, and afterwards evaporated to dryness. The titanium purification was modified from the two-step protocol described in Zhang et al. (2011). To avoid using large amounts of DGA resin, the order of the chromatographic steps was inverted (Protocol I). The first column was custom-made from a heat-shrinkable Teflon tube and the resin bed (0.6 cm inner diameter × 4 cm length) was filled with 1.1 cm^3 chloride-form Bio-Rad AG1-X8 resin (200–400 mesh). The samples were loaded in 0.5 ml 4 M HF and the matrix (mostly alkali and transition metals, including Fe) was removed with additional 9.5 ml 4 M HF. Titanium was then eluted in 5 ml 6 M HCl + 0.01 M HF together with Ca, V, Zr, Hf, Al, Sr, Ba and Mg. The samples were dissolved in 16 M HNO_3 and dried, twice, to remove the remaining traces of HF and HCl. The second column, also made from heat-shrinkable Teflon (0.45 cm diameter × 1.3 cm length), was filled with 0.2 cm^3 Eichrom DGA resin (50–100 μm particle size). The samples were loaded in 100 μl 12 M HNO_3 and the remaining matrix elements were removed by addition of 900 μl 12 M HNO_3. The final Ti cut was collected in 600 μl MilliQ H_2O (Supplementary Table S1). After chemistry, the purified samples were evaporated and organic particles derived from the resins were decomposed by fluxing with 16 M HNO_3 at about 120 °C overnight.

Protocol I was tested with (terrestrial) geological reference materials and Ti yields of typically >90% were achieved. However, some Ti elution cuts still contained small amounts of Fe (Fe/Ti ≈ 0.1–1). Furthermore, the Ti yields for some chondrite samples were as low as 20% (data not included in this study). Titanium was likely lost after the first column due to the fluoride formation of remaining Mg. Although the double spike is able to correct for isotope fractionations induced by incomplete recovery, a second protocol (Protocol II) was set up for extraterrestrial samples to increase the Ti yields. As Fe competes with Ti on the DGA resin and the capacity of the resin is easily exceeded by the loaded amount of sample matrix, Fe was first removed from the matrix by a preceding column (0.6 cm diameter × 4 cm length) using AG1-X8 resin. The samples were loaded in 0.5 ml 6 M HCl, and Ti (plus other matrix elements) was immediately collected with in total 6 ml 6 M HCl, while Fe remained on the resin. After evaporation, the samples were dissolved in 12 M HNO_3 and subjected to the DGA column to remove especially Ca, Cr and V as described above. In the last step of Protocol II, the Mg-free sample cuts were finally passed through an AG1-X8 column with 4 M HF (Supplementary Table S2). Organic compounds in the dried samples that were released from the resins were digested in 16 M HNO_3 at about 120 °C overnight. Typical Ti blanks for the both column chemistry protocols were < 2 ng, which is negligible compared to the loaded amount of natural Ti (≥1.5 μg) and the typical Ti yield after chemistry (≥ 80%) (Supplementary Table S6).

2.2.3. Ti reference material and ^{47}Ti-^{49}Ti double spike

A reference material for Ti isotope analyses (hereafter referred as IPGP-Ti) was prepared from a Ti ICP standard solution (1000 μg/ml PlasmaCal, SCP Science, Lot SC7186430). IPGP-Ti was diluted to about 10 μg/ml and stored in 1 M HNO_3 + 0.01 M HF.

The enriched spikes were purchased from CortecNet (Voisins-le-Bretonneux, France): ^{47}Ti (95.7%) and ^{49}Ti (93.3%). The single spikes were digested in about 20 M HF. Optimal double spike composition and double spike to sample ratio were calculated using the double spike toolbox (Rudge et al., 2009). The two single spikes were mixed accordingly and the double spike was further diluted to a concentration of about 5 μg/ml Ti (^{47}Ti + ^{49}Ti), stored in 1 M HNO_3 + 0.01 M HF. The ^{47}Ti-^{49}Ti double spike was calibrated relative to IPGP-Ti. First, pure solutions of IPGP-Ti and double spike were measured separately to estimate their Ti isotope abundances. Chromium was used as a dopant to internally correct for instrumental mass bias with a fixed ^{53}Cr/^{52}Cr ratio of 0.1134 (de Laeter et al., 2003). In a second step, nine aliquots of IPGP-Ti with increasing double spike proportions were analyzed three times each. The preliminary $\delta^{49/47}$Ti values of IPGP-Ti were calculated by conducting double spike inversion for the measured isotopic ratios, and the isotopic composition of the ^{47}Ti-^{49}Ti double spike can be estimated by mass-dependently adapting the $\delta^{49/47}$Ti value of IPGP-Ti to 0‰. At double spike to sample ratios >0.60, the calculated $\delta^{49/47}$Ti values of IPGP-Ti aliquots deviates from 0‰. Therefore, the optimized double spike proportion in the mixture of double spike and IPGP-Ti ranges from 0.42 to 0.60. The calculated Ti isotopic composition of the IPGP-Ti standard and ^{47}Ti-^{49}Ti double spike are provided in Supplementary Table S3.

The double spike method has been in use since the 1960s (e.g., Dodson et al., 1969; Compston and Oversby, 1969; Russell et al., 1978; Rudge et al., 2009). Niederer et al. (1985) employed a double spike to measure the Ti isotopic composition of meteorites and terrestrial rocks. As explained by Niederer et al. (1985), in order to determine the absolute Ti isotopic composition of unknown samples, a gravimetric stoichiometry of the used double spike is necessary. The method monitors the Ti isotopic fractionations in the samples relative to the assumed normalization value for ^{46}Ti/^{48}Ti (Niederer et al., 1985) or ^{49}Ti/^{47}Ti (here) in the Ti standard, and only the differences in Ti isotopic fractionations are absolute.

2.2.4. Mass spectrometry

The dried Ti elution cuts after chemistry were dissolved in 0.5 M HNO_3 + 0.0015 M HF for analyses on the Thermo Scientific Neptune Multi-Collector Inductively-Coupled-Plasma Mass-Spectrometer (MC-ICP-MS) housed at IPGP. Traces of HF were used to stabilize Ti in dissolution. Sample solutions were introduced via an APEX HF desolvating nebulizer (Elemental Scientific Inc., USA), used without spare gas and with an uptake rate of 70 μl/min. Typical sensitivity was 17–19 V on ^{48}Ti$^+$ (using a 10^{11} Ω

resistor) for a solution containing 300 ppb of Ti measured under medium mass resolution (M/ΔM ≈ 5800). Two sample introduction protocols were used to calibrate the OL-Ti standard relative to the IPGP-Ti standard, i.e., 1 ppm solution introduced via a quartz dual cyclonic spray chamber and 300 ppb solution via an APEX HF desolvating nebulizer. Between two analyses, Ti was washed out by a first rinse with 1.2 M HNO_3 + 0.0015 M HF, followed by a second rinse with 0.5 M HNO_3 + 0.0015 M HF, until a typical background of 2–5 mV on $^{48}Ti^+$ was reached.

Data acquisition consisted of 100 cycles with an integration time of 8 s. The signals of $^{44}Ca^+$, $^{46}Ti^+$, $^{47}Ti^+$, $^{48}Ti^+$, $^{49}Ti^+$ and $^{50}Ti^+$ were simultaneously detected in static mode. $^{44}Ca^+$ intensities were used to correct for interferences of ^{46}Ca and ^{48}Ca on ^{46}Ti and ^{48}Ti, respectively. The instrumental mass fractionation factor determined for Ti for each measurement cycle by double spike data reduction (see below) was applied to the natural Ca isotopic ratios ($^{44}Ca/^{46}Ca = 657.03$ and $^{44}Ca/^{48}Ca = 11.14$; de Laeter et al., 2003), and the estimated $^{46}Ca^+$ and $^{48}Ca^+$ intensities were subtracted from the total signals on masses 46 and 48. To avoid measurements in dynamic mode, signals of $^{51}V^+$ and $^{52}Cr^+$ were not monitored and interferences of ^{50}V and ^{50}Cr on ^{50}Ti could not be corrected. Thus, ^{50}Ti was not used for further data reduction. Due to the use of a quartz injector and plasma torch in combination with HF, isobaric interferences from silicon oxides and fluorides, e.g., $^{28}Si^{16}O^+$ on $^{44}Ca^+$, $^{30}Si^{16}O^+$ on $^{46}Ti^+$ and $^{28}Si^{19}F^+$ on $^{47}Ti^+$, occurred. These polyatomic interferences were resolved in medium resolution (M/ΔM ≈ 5800) and the interference-free signals were measured at the low mass of the peaks for masses 44, 46 and 48 (Supplementary Table S4). Polyatomic interferences on $^{48}Ti^+$ ($^{30}Si^{18}O^+$ and $^{29}Si^{19}F^+$) and $^{49}Ti^+$ ($^{30}Si^{19}F^+$) were found negligible and data were acquired at center peaks (Supplementary Fig. S1).

Supplementary data associated with this article can be found, in the online version, at https://doi.org/10.1016/j.gca.2018.06.016.

2.2.5. Data reduction and notation

Data reduction was accomplished with the IsoSpike software (Creech and Paul, 2015). Signals of ^{46}Ti, ^{47}Ti, ^{48}Ti and ^{49}Ti after Ca correction were used for double spike inversion. Within each analysis, statistic outliers among 100 cycle measurements that scatter beyond 2-sigma were identified and removed from double spike inversion. The measured results for the samples without Ti isotopic anomaly are supposed to follow:

$$R^{i/k}_{sample} = R^{i/k}_{standard}\left(\frac{m_i}{m_k}\right)^{\alpha} \quad (1)$$

$$R^{i/k}_{measured} = \left[(1-\lambda)R^{i/k}_{standard}\left(\frac{m_i}{m_k}\right)^{\alpha} + \lambda R^{i/k}_{spike}\right]\left(\frac{m_i}{m_k}\right)^{\beta} \quad (2)$$

with i the Ti isotope of interest (e.g., ^{46}Ti, ^{48}Ti and ^{49}Ti), and k the Ti isotope used as the denominator (e.g., ^{47}Ti), $R^{i/k}_{measured}$, $R^{i/k}_{standard}$ and $R^{i/k}_{spike}$ the isotopic ratios of measured mixture, standard and spike, respectively, and m the atomic mass of isotope i or k. α is the mass-dependent Ti isotopic fractionation in the sample relative to standard, and β represents the instrumental mass bias. λ is the mass proportion of isotope k from the spike in the sample-double spike mixture.

However, since chondrites exhibit isotopic anomalies on ^{46}Ti, ^{48}Ti and ^{50}Ti (Niederer et al., 1985; Trinquier et al., 2009; Zhang et al., 2012; Niemeyer and Lugmair, 1981; Niemeyer and Lugmair, 1984), their stable isotopic compositions may deviate from the terrestrial mass-dependent fractionation line on which the reference material IPGP-Ti lies (Greber et al., 2017a). To account for this deviation, the assumed normalization values of IPGP-Ti have to be adapted for the anomalies for each individual sample and the $\delta^{49/47}Ti$ values of chondrites have to be reduced relative to the adapted normalization values:

$$R^{i/k}_{standard-adapted} = R^{i/k}_{standard}\left(1 + \varepsilon^{i/k}/10^4\right) \quad (3)$$

with $\varepsilon^{i/k}$ the mass-independent Ti isotopic fractionation on the isotopic ratio of isotope i to k and $R^{i/k}_{standard-adapted}$ the adapted normalization values for the IPGP-Ti standard. After this, the adapted normalization values of IPGP-Ti would lie on the same mass-dependent fractionation line as the samples showing isotopic anomalies. The double spike inversion was conducted on the results of the double spiked samples to determine the mass-dependent Ti isotopic fractionations by replacing $R^{i/k}_{standard}$ with $R^{i/k}_{standard-adapted}$ in Eq. (2). In this study, mass-independent Ti isotopic data from Trinquier et al. (2009) and Zhang et al. (2012) were used. For the samples without available mass-independent isotopic data, the average values of the corresponding meteorite groups were used. This protocol is principally the same as the one used for Ba isotopes in Eugster et al. (1969), i.e., the results of the un-spiked samples were normalized onto the assumed values of the Ba standard, and the normalized un-spiked sample compositions and the results from the double spiked samples were combined to run a double spike inversion to calculate the mass-dependent Ba isotopic fractionations.

While the ^{47}Ti-^{49}Ti double spike has been used in this study, the analytical results here have been converted into $^{49}Ti/^{47}Ti$ ratios since (i) this data reporting manner discriminates mass-dependent Ti isotopic fractionations from isotopic anomalies on ^{46}Ti and ^{48}Ti (Trinquier et al., 2009; Zhang et al., 2012) and (ii) a delta notation on $^{49}Ti/^{47}Ti$ ratio has been adopted by the most recent studies on Ti stable isotopic variations (Millet and Dauphas, 2014; Millet et al., 2016; Greber et al., 2017a). As such, the data are reported in the δ-notation relative to IPGP-Ti for $^{49}Ti/^{47}Ti$ ratio:

$$\delta^{49/47}Ti_{IPGP-Ti} = \left[\frac{(^{49}Ti/^{47}Ti)_{sample}}{(^{49}Ti/^{47}Ti)_{IPGP-Ti}} - 1\right] \times 1000 \quad (4)$$

The isotopic differences between Ti standards from different laboratories are expressed in ‰:

$$\Delta^{49/47}Ti_{standard1-standard2} = \left[\frac{(^{49}Ti/^{47}Ti)_{standard1}}{(^{49}Ti/^{47}Ti)_{standard2}} - 1\right] \times 1000 \quad (5)$$

The spiked IPGP-Ti standard was measured after every second sample. After the $\delta^{49/47}Ti$ values of both IPGP-Ti standard and samples were calculated by double spike

inversion, the $\delta^{49/47}$Ti values for samples were further normalized against the average $\delta^{49/47}$Ti values of the preceding and succeeding bracketing IPGP-Ti standards. This normalization can reduce the effects of (i) the short-term fluctuations that probably come from instrumental instability, and (ii) the different molecular interferences between sessions as the results of the small tailing effects from $^{30}Si^{18}O^+$, $^{29}Si^{19}F^+$ and $^{30}Si^{19}F^+$.

For the data set of geological reference materials, the long-term external precision was estimated by calculating the 'pooled' standard deviation ($2s_p$), i.e., ± 0.027‰ on the $^{49}Ti/^{47}Ti$ ratio:

$$s_P = \sqrt{\frac{\sum_{i=1}^{k}(n_i-1)s_i^2}{\sum_{i=1}^{k}(n_i-1)}} \quad (6)$$

where n_i is the number of repeated measurements of each sample i and s_i^2 their variance. This suggests that the upper limit of the typical uncertainty on the measured $\delta^{49/47}$Ti is ± 0.027‰. Since each sample analysis has been bracketed by the analyses of the IPGP-Ti standard, the short-term precision was quoted here, i.e., using the 2se values of the measurement duplicates as the analytical uncertainties on the average $\delta^{49/47}Ti_{IPGP\text{-}Ti}$ values of the rock standards and chondrites. Since the Ti isotopic anomalies of chondrites have been previously determined with a precision of ± 0.05 on ε^{46}Ti (2se) in Trinquier et al. (2009) and Zhang et al. (2012), the isotopic anomaly correction would not significantly affect the reported analytical uncertainties for the studied chondrites.

3. RESULTS

3.1. Tests for the possible sources of analytical artifacts

3.1.1. Sample digestion

Incomplete sample digestion may cause biased Ti isotope data, when minerals inert towards chemical attacks bear highly fractionated Ti isotopic compositions. Possible effects of the digestion methods on the Ti isotope measurements were tested by digesting aliquots of powders of several samples by two or more of the above described methods. In general, the $\delta^{49/47}$Ti values are in excellent agreement within analytical uncertainty (Fig. 1). Isna (CO3.8) and Allende (CV3), however, cannot be reproduced within analytical uncertainty between different aliquots (Fig. 1). Niederer et al. (1985), Trinquier et al. (2009) and Zhang et al. (2012) have shown that CAIs have considerably different Ti isotopic anomalies compared to chondrules and matrix. Therefore, CO- and CV-type chondrites that are enriched in CAIs are particularly prone to isotopic heterogeneities, and isotope anomaly data may vary amongst sample aliquots, based on the proportion of CAIs. As there is no systematic trend in the $\delta^{49/47}$Ti data with digestion method and the dissolution aliquots of the Isna and Allende meteorites were dissolved from the powders crushed from different sample pieces, the offset may be a result of whole-rock heterogeneity rather than of incomplete digestion.

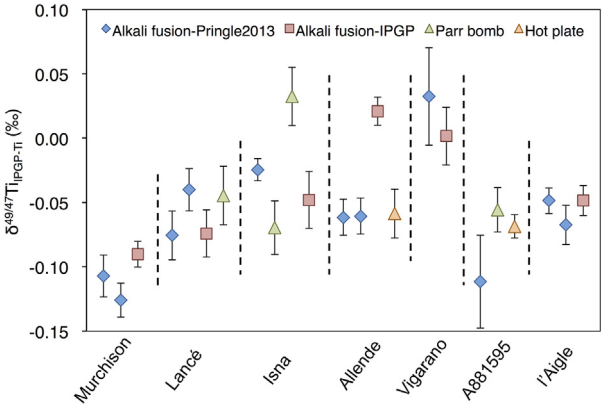

Fig. 1. Titanium isotopic composition of sample aliquots digested by different methods. Error bars indicate 2se uncertainties (see Supplementary Table S6).

3.1.2. Titanium recovery

Column yields for *Protocol II* were >80% for all samples, and in some cases the recovery was twice as large as for *Protocol I* (Supplementary Fig. S2A). Within an external measurement precision of ±0.03–0.08‰ for chondrite samples, aliquots processed by using the two protocols have indistinguishable $\delta^{49/47}$Ti values (Supplementary Fig. S2B). Thus, Ti isotope data acquired for samples with column yields as low as ~40% were included in this study. In the case of the Allende chondrite, the recovery rates of all aliquots were >80%. The higher $\delta^{49/47}$Ti value for the dissolution aliquot purified following *Protocol II* is therefore likely the result of sample heterogeneity (Supplementary Fig. S2). As such, the similarity between low- and high-yield replicates demonstrates that the double spike method here can correct for the incomplete titanium recovery as low as 40%. For samples with high Mg concentrations, such as chondrites, the three-step chromatographic protocol is recommended in order to achieve a high Ti recovery. For terrestrial igneous rocks, however, the shorter two-step protocol is sufficient with Ti yields > 90% (Table 1), while lowering the procedure blank and the amount of time required for sample purification.

3.1.3. Sample impurity

Aliquots of IPGP-Ti were doped with varying amounts of Fe, Ca and Si to test for isobaric and non-spectral matrix effects. It appears that non-spectral matrix effects of Fe on the measured Ti isotopic ratios are negligible for Fe/Ti ratios ≤ 10 (Fig. 2). Isobaric interferences of Ca can successfully be corrected for Ca/Ti ratios ≤ 0.1. Significant amounts of Si (Si/Ti > 0.1) cause systemically lower $\Delta^{49/47}Ti_{IPGP\text{-}Ti}$ values due to the tailing effects of $^{28}Si^{19}F^+$ (Fig. 2). The effect of Si on the Ti measurements might be relevant especially for the samples digested by alkali fusion, as dissolved Si remains in solution. However, different digestion methods result in indistinguishable $\Delta^{49/47}Ti_{IPGP\text{-}Ti}$ values. Furthermore, small amounts of Si from the quartz glass injector and torch are considered to produce Si/Ti ratios ≪ 0.1 (Supplementary Fig. S1; Supplementary Table S5). Thus, the effects of the tested impurities after chromatographic purification are negligible on the $\delta^{49/47}$Ti values in this study.

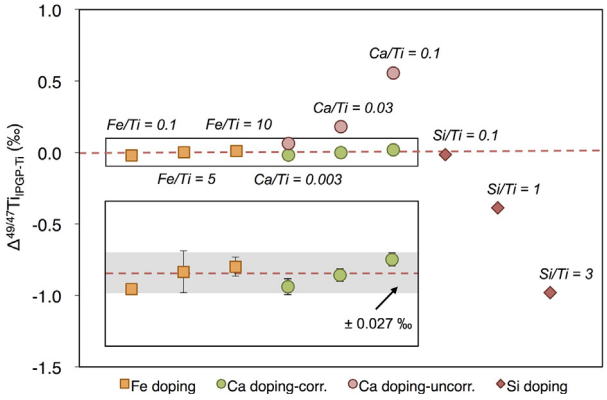

Fig. 2. Results of matrix doping. For Ca doping, uncorrected (green) and corrected data (pink) are shown. The isobaric interferences from Si doping were not corrected, which can lead to lower $\delta^{49/47}Ti_{IPGP\text{-}Ti}$ values when Si/Ti is > 0.1. Note: Si/Ti is ≪ 0.1 for the unknown samples in this study after chromatographic purification. Error bars indicate 2se uncertainties (smaller than symbol size). The inset is the zoom-in for the box field. The grey bar shows the typical precision of ± 0.027‰ for the samples with only one or two duplicates. (For interpretation of the references to colour in this figure legend, the reader is referred to the web version of this article.)

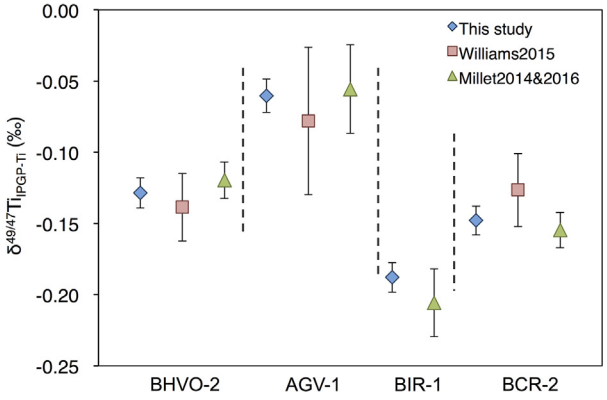

Fig. 3. Comparison of results from reference materials (AGV-1, BHVO-2, BCR-2 and BIR-1) in this study with the literature data (Williams, 2015; Millet and Dauphas, 2014; Millet et al., 2016).

Normally, the isobaric interferences from $^{46}Ca^{+}$ and $^{48}Ca^{+}$ on $^{46}Ti^{+}$ and $^{48}Ti^{+}$, respectively, can be corrected by monitoring the intensity of $^{44}Ca^{+}$ and applying the natural Ca isotopic ratios. However, if a small amount of the unnatural and highly isotopically fractionated Ca was present in the used double spike, this Ca correction manner might lead to either the over- or under-correction of the Ca isobaric interferences. A systematic drift on the $\delta^{49/47}Ti$ values would be expected upon a fact that: The spiked samples were cleaned after chromatographic purification, but the spiked bracketing IPGP-Ti standard was not. To test this, we measured a spiked IPGP-Ti solution passed through the DGA column against the spiked bracketing IPGP-Ti standard, which provide a resolvable $\Delta^{49/47}Ti = +0.022 \pm 0.009‰$ (2se, n = 9) (Table 1). The measurements on the used double spike show that the intensities are ≈ 4 mV on $^{44}Ca^{+}$ while ≈ 18–20 V on $^{47}Ti^{+}$ and $^{49}Ti^{+}$. Therefore, we suggest here that the small drift is likely the result of a remnant of the isotopically non-natural Ca that came in as part of the isotope enrichment procedure. This systematic drift is unlikely to alter the Ti isotopic differences between samples within an individual laboratory. Nonetheless, if aiming for high-precision inter-laboratory comparison, the purification on both the samples and bracketing IPGP-Ti standard would be necessary. Thus, all the $\delta^{49/47}Ti$ values in this study were corrected for this drift with error propagation.

3.2. Inter-laboratory comparison

While the measurements with spray chamber show a $\delta^{49/47}Ti_{IPGP\text{-}Ti} = -0.158 \pm 0.008‰$ (2se) for the OL-Ti standard, the analyses with Apex provide a slightly higher $\delta^{49/47}Ti_{IPGP\text{-}Ti}$ value of $-0.140 \pm 0.011‰$ (2se). Here the latter value is preferred since all the samples have been measured with Apex. After the correction of the Ca effects from double spike in Section 3.1.3, resolvable Ti isotopic variations can be observed for BIR-1 ($\delta^{49/47}Ti_{IPGP\text{-}Ti} = -0.188 \pm 0.010‰$, 2se), BCR-2 ($\delta^{49/47}Ti_{IPGP\text{-}Ti} = -0.148 \pm 0.010‰$, 2se), BHVO-2 ($\delta^{49/47}Ti_{IPGP\text{-}Ti} = -0.129 \pm 0.011‰$, 2se) and AGV-1 ($\delta^{49/47}Ti_{IPGP\text{-}Ti} = -0.060 \pm 0.012‰$, 2se) (Fig. 3; Table 1; Supplementary Table S6). Replicates of the rock standards imply that our method is able to resolve the subtle Ti stable isotopic fractionation in nature, i.e., ~0.010‰ on $\delta^{49/47}Ti_{IPGP\text{-}Ti}$ within 95% confidence interval. These values for the rock standards BIR-1, BCR-2, BHVO-2 and AGV-1 match well with the reported values in Williams (2015), Millet and Dauphas (2014) and Millet et al. (2016) within errors (Fig. 3; Table 1).

3.3. Stable Ti isotopic compositions of bulk chondrites

The $\delta^{49/47}Ti_{IPGP\text{-}Ti}$ values of individual chondrite samples vary within a range of 0.176‰ ($\delta^{49/47}Ti_{IPGP\text{-}Ti}$ of $-0.162 \pm 0.011‰$ to $+0.014 \pm 0.024‰$; Table 2). Nonetheless, the average values for individual chondrite groups (CI, CM, CO, CV, CR, CH, CK, L, LL, EL and EH) are indistinguishable within the analytical uncertainty ($\delta^{49/47}Ti_{IPGP\text{-}Ti} = -0.070 \pm 0.015‰$, 2se, n = 11) (Table 2; Supplementary Table S6). Furthermore, the average $\delta^{49/47}Ti_{IPGP\text{-}Ti}$ value of the individual chondrite samples ($\delta^{49/47}Ti_{IPGP\text{-}Ti} = -0.069 \pm 0.018‰$, 2se, n = 22) is similar to the average chondrite value from Williams (2015) ($\delta^{49/47}Ti_{IPGP\text{-}Ti} = -0.090 \pm 0.028‰$, 2se, n = 6), while slightly heavier when compared to the bulk silicate Earth estimate from Millet et al. (2016) ($\delta^{49/47}Ti_{IPGP\text{-}Ti} = -0.133 \pm 0.014‰$, 2se; n = 26) and the chondrite average from Greber et al. (2017a) ($\delta^{49/47}Ti_{IPGP\text{-}Ti} = -0.132 \pm 0.015‰$, 2se; n = 16 with 4 CC, 3 EC and 9 OC) (Fig. 4; Supplementary Table S7).

4. DISCUSSION

4.1. Homogeneous Ti stable isotopic compositions of chondrites

While the rock standards show similar $\delta^{49/47}Ti_{IPGP\text{-}Ti}$ values in this study, Williams (2015) and Millet and

Dauphas (2014), the chondrites from this study and Williams (2015) are ~0.040–0.060‰ higher in $\delta^{49/47}Ti_{IPGP\text{-}Ti}$ values than those from Greber et al. (2017a). The presence of this inter-laboratory discrepancy motivated us to carry out a series of tests to clarify the possible sources of analytical artifacts in Section 3.1, though no reason for such a discrepancy was apparent. However, it is unquestionable that the eleven studied individual chondrite groups are homogenous in Ti stable isotopic composition.

The Ti stable isotopic homogeneity for bulk chondrites with varying degrees of aqueous alteration and metamorphism implies that Ti isotopes are not affected by these processes. In contrast with the Ti stable isotopic homogeneity for bulk chondrites, the CAIs in chondrites are characterized by much larger mass-dependent Ti isotopic variations. Seven CAI samples in Niederer et al. (1985) show an enrichment in heavy Ti isotopes compared to terrestrial rocks (+0.1‰/amu to +1.3‰/amu), and forty-nine CAIs from Allende chondrites have both positive and negative $\delta^{49/47}Ti_{IPGP\text{-}Ti}$ values with an average $\delta^{49/47}Ti_{IPGP\text{-}Ti}$ value of +0.20 ± 0.33‰ (2se, n = 49; Davis et al., 2018). On average, the CAIs in CV-type chondrites can contain 15–20% of the total Ti (Hezel and Palme, 2007). Thus, the similarity of Ti stable isotopic composition across carbonaceous chondrite groups implies that CAIs in chondrites are, on average, not markedly isotopically different from other non-CAI components in Ti, even if a $\delta^{49/47}Ti_{IPGP\text{-}Ti}$ range of ~7‰ has been observed in CAIs in Davis et al. (2018).

The large variation on $\delta^{49/47}Ti_{IPGP\text{-}Ti}$ for individual CAIs suggests that the condensation and evaporation processes that formed the CAIs in the early solar nebula can significantly fractionate Ti stable isotopes (Niederer et al., 1985; Zhang et al., 2014; Davis et al., 2018). As a refractory lithophile element, most Ti would enter the condensates after 5% of CI chondritic composition was condensed (Davis and Richter, 2003). The primary Ti-bearing condensates, e.g., perovskite and hibonite, can further equilibrate with the surrounding liquids or gases during the cooling processes of the early solar nebula. This re-equilibration would lead to the forming of other Ti-bearing components, e.g., pyroxenes or mesostasis in the chondrules of carbonaceous and ordinary chondrites (Hezel and Palme, 2007), or the sulfides or metals of enstatite chondrites (Keil, 1969). The aggregation of the varying components can result in various types of chondrites with bulk TiO_2 contents ranging from ~0.05 wt% (EH-type) to ~0.15 wt% (CV-type) (Supplementary Table S6). Thus, the Ti stable isotopic homogeneity among eleven chondrite groups may imply that chondrites have inherited the average stable isotopic composition of the early condensed Ti through the efficient re-equilibration between the primary refractory condensates and liquids or gases in the solar nebula.

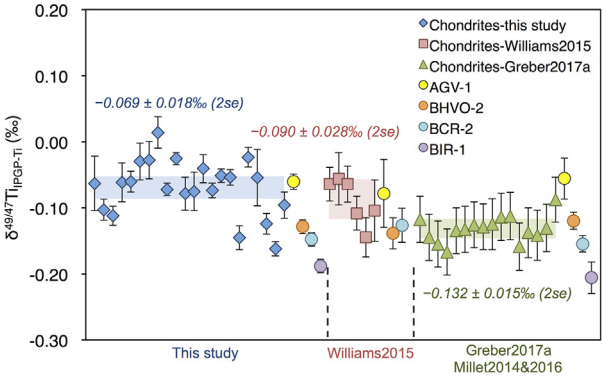

Fig. 4. $\delta^{49/47}Ti_{IPGP\text{-}Ti}$ values of chondrites and rock standards in this study. The chondrite and rock standard data from Williams (2015), Greber et al. (2017a), Millet and Dauphas (2014) and Millet et al. (2016) are shown for comparison. All the data have been rescaled onto the IPGP-Ti standard with error propagation. The average of each group of data is indicated with 2se uncertainty.

4.2. Constraints on the Ca stable isotopic variations in bulk chondrites

While there is a Ti stable isotopic homogeneity for bulk chondrites, the CI-, CM-, CV- and CR-type chondrites exhibit lower $\delta^{44/40}Ca_{NIST\ SRM\ 915a}$ values from +0.27 ± 0.04‰ to +0.79 ± 0.09‰ (2se) when compared to those of CO-type chondrites (+0.97 ± 0.18‰, 2se), and ordinary and enstatite chondrites (+0.91‰ to +0.97‰) (Valdes et al., 2014; Simon and DePaolo, 2010; Amsellem et al., 2017; Huang and Jacobsen, 2017). These observations demonstrate that the Ca isotopes behave differently from Ti isotopes in bulk chondrites.

4.2.1. Inheritance from CAIs?

While multiple CAIs are on average similar to bulk chondrites with respect to Ti stable isotopes (Davis et al., 2018; Niederer et al., 1985; Simon et al., 2017), the CAIs from Allende are mostly isotopically lighter in Ca ($\delta^{44/40}Ca_{NIST\ SRM\ 915a}$ down to −10.34‰) than the bulk values of Allende ($\delta^{44/40}Ca_{NIST\ SRM\ 915a}$ = −0.61‰ to −0.27‰), Allende chondrules ($\delta^{44/40}Ca_{NIST\ SRM\ 915a}$ = +0.91‰ to +1.06‰; Amsellem et al., 2017) and ordinary/enstatite chondrites (+0.91‰ to +0.97‰) (Niederer and Papanastassiou, 1984; Huang et al., 2012; Huang and Jacobsen, 2017; Simon et al., 2017; Valdes et al., 2014; Simon and DePaolo, 2010; Amsellem et al., 2017). In a gas phase above silicate liquids, Ca is present as Ca^0, while Ti mainly occurs as TiO_2 (Zhang et al., 2014), though TiO is also present in small proportions (De Maria et al., 1971). The smaller relative mass difference per atomic mass unit of $Ti^{49}O_2/Ti^{47}O_2$ with respect to Ca^{44}/Ca^{40} reduces mass-dependent isotopic fractionation of the former during evaporation (Zhang et al., 2014; Simon et al., 2017). Nonetheless, in contrast with the canonical Ti stable isotope records, the light Ca isotopic compositions for CAIs imply that a significant fraction of isotopically heavy Ca has been removed from the CAI source materials (Niederer and Papanastassiou, 1984; Huang et al., 2012).

The CAIs may contribute significantly to the inventory of refractory lithophile elements in bulk CV-type chondrites, as attested by the similar Rare Earth Element (REE) pattern between Allende (CV3) and Group II CAIs (Huang et al., 2012). Thus, Ca isotope variations in CV-type chondrites may be controlled by the modal abundance of isotopically light CAIs. If so, a correlation between CAI

abundances and Ca stable isotopic compositions would be expected among different types of chondrites. As documented in Hezel and Palme (2008), the abundances of refractory inclusions in individual carbonaceous chondrite groups follow an order of CI ≈ CR < CO < CM < CV, with CI- and CR-type chondrites containing almost no CAIs. Following this logic, CI- and CR-type chondrites that are CAI-free should have heavier Ca stable isotopic composition compared to the CO- and CM-type chondrites, which is not the case (Valdes et al., 2014; Simon and DePaolo, 2010; Amsellem et al., 2017). Therefore, other mechanisms are needed to explain variation in stable isotopic composition of Ca in bulk chondrites.

4.2.2. Parent-body aqueous alteration?

A major chemical difference between Ca and Ti is that Ca is very mobile during aqueous alteration while Ti is not (Van Baalen, 1993). Oxygen isotopic variations between CI-, CR- and CM-type chondrites show that they have experienced variable degrees of aqueous alteration in their parent bodies (Clayton et al., 1988; Clayton and Mayeda, 1999; Rowe et al., 1994; Weisberg et al., 1993). As addressed by Clayton and Mayeda (1999), the slopes (S) of individual carbonaceous chondrite groups on a triple oxygen isotope plot (relative variations of the $^{17}O/^{16}O$ ratios versus the $^{18}O/^{16}O$ ratios) can be used as an indicator of the degrees of aqueous alteration ($S_{CV} \approx 1$, $S_{CM+CO} \approx 0.70$, $S_{CR+CH} \approx 0.59$ and $S_{CI} \approx 0.5$; Clayton and Mayeda, 1999). This idea follows a logic that the anhydrous minerals of carbonaceous chondrites plot along a line with $S \approx 1$ (Clayton et al., 1973), while aqueous alteration induces isotope fractionations varying along lines with $S \approx 0.5$ (Clayton and Mayeda, 1999). Thus, an index for increasing aqueous alteration can be defined from oxygen isotopes in the order CV < CO < CM < CI ≤ CR.

The contribution from CAIs on the Ca stable isotopic inventory of carbonaceous chondrites can be subtracted by using the CAI abundance and chemical composition data from Hezel and Palme (2007, 2010), and temporarily assuming $\delta^{44/40}Ca_{NIST\ SRM\ 915a} = -0.9‰$ and CaO = 18 wt% for CAIs in average. After the subtraction of the contribution of CAIs, CV-, CO- and CM-type chondrites exhibit similar Ca isotopic compositions as that of ordinary or enstatite chondrites (Valdes et al., 2014; Amsellem et al., 2017), but CR- and CI-type chondrites still have resolvable lighter Ca isotopic ratios (Fig. 5). This observation indicates that the Ca stable isotopic inventory in CR- and CI-type chondrites may have been altered by parent-body aqueous alteration. Similar interpretations have been given to explain the different Mg isotopic composition of CI and CR chondrites from other carbonaceous chondrite groups (Hin et al., 2017), as corroborated by their high $^{18}O/^{16}O$ ratios. This interpretation is supported by the fact that the water-soluble phases from CI-type chondrite Orgueil extracted with boiling water contain up to nearly 50% of the total Ca and the main water-soluble Ca carriers are the Ca-sulfates and carbonates formed by aqueous activity in the parent body (Fredriksson and Kerridge, 1988).

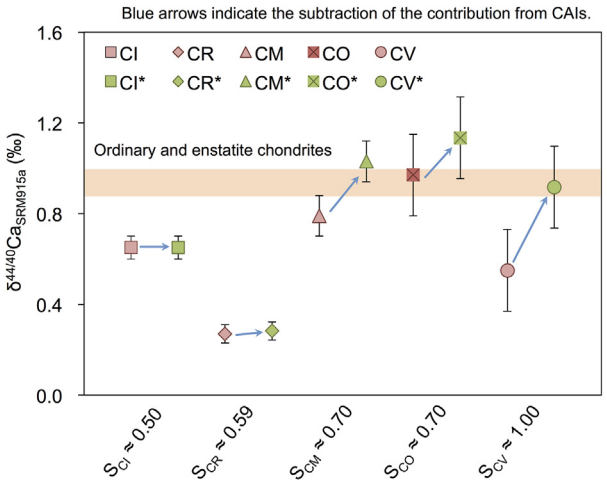

Fig. 5. Diagram showing the subtraction of CAIs on the Ca stable isotopic inventory of CI-, CR-, CM-, CO- and CV-type chondrites. This subtraction was conducted by a mass balance using parameters shown in Supplementary Table S8 (i.e., the blue arrows), by assuming that CAIs in average have a CaO content of 18 wt% and a $\delta^{44/40}Ca_{NIST\ SRM\ 915a}$ value of −0.9‰. The pink labels represent the original Ca stable isotopic values while the green ones stand for the values after subtraction of CAIs. The slopes of chondrite groups defined on the triple oxygen isotope plot from Clayton and Mayeda (1999) are indicated at the bottom. The $\delta^{44/40}Ca_{NIST\ SRM\ 915a}$ value of ordinary and enstatite chondrites in Valdes et al. (2014) is shown as an orange bar. (For interpretation of the references to colour in this figure legend, the reader is referred to the web version of this article.)

5. CONCLUSIONS

Eleven chondrite groups (CI, CM, CO, CV, CR, CH, CK, L, LL, EL and EH-type) exhibit indistinguishable Ti stable isotopic compositions with an average $\delta^{49/47}Ti_{IPGP\text{-}Ti}$ of −0.070 ± 0.015‰ (2se). This homogeneity corroborates that CAIs on average should be similar to the bulk chondrites for Ti stable isotopes, and chondrites have inherited the average Ti isotopic composition of the solar system through the condensation sequence. In contrast, the large Ca stable isotopic variations in bulk chondrites are likely the combining results of (i) the incorporation of CAIs and (ii) aqueous alteration. Future characterization of the carrier phases for the light Ca stable isotopic signatures among non-CAI chondritic components will be helpful to testify whether chondrites have also sampled the average Ca stable isotopic composition from the early condensates in the early solar nebula, which has been demonstrated for Ti.

ACKNOWLEDGEMENTS

We thank Julien Moureau, Pascale Louvat, Jessica Dallas and Pierre Burckel for maintaining the MC-ICP-MS and Q-ICP-MS at IPGP, John Creech for his help with IsoSpike software, and Marc-Alban Millet for sharing the OL-Ti standard. Dimitri Papanastassiou, Justin Simon and two anonymous reviewers are greatly appreciated for their constructive comments on our

manuscript. FM acknowledges funding from the European Research Council under the H2020 framework program/ERC grant agreement #637503 (Pristine). FM and MC thank financial support from the ANR through the Cradle project and the UnivEarthS Labex program at Sorbonne Paris Cité (ANR-10-LABX-0023 and ANR-11-IDEX-0005-02). Parts of this work were supported by IPGP multidisciplinary program PARI, and by Region Île-de-France SESAME Grant no. 12015908. We are also indebted to Joseph Boesenberg and Denton Ebel (American Museum of National History, New York), Timothy McCoy (US National Museum of Natural History, Smithsonian Institution, Washington DC), Caroline Smith (The Natural History Museum, London), Alex Bevan (Western Australian Museum, Perth), Jim Karner and Carl Agee (University of New Mexico, Albuquerque), Ludovic Ferriere (Naturhistorisches Museum, Vienna), Philip Heck (The Field Museum, Chicago), Meenakshi Wadhwa (Arizona State University, Tempe), Cecilia Satterwhite (NASA Johnson Space Center, Houston) and the Comité de Gestion (Museum Nationale d'Histoire Naturelle, Paris) for their generous donations of meteorite samples for this work and their confidence in our analytical and scientific capabilities.

REFERENCES

Anders E. and Grevesse N. (1989) Abundances of the elements: meteoritic and solar. *Geochim. Cosmochim. Acta* **53**, 197–214.

Amsellem E., Moynier F., Pringle E. A., Bouvier A., Chen H. and Day J. M. (2017) Testing the chondrule-rich accretion model for planetary embryos using calcium isotopes. *Earth Planet. Sci. Lett.* **469**, 75–83.

Birck J. L. and Allègre C. J. (1985) Evidence for the presence of ^{53}Mn in the early solar system. *Geophys. Res. Lett.* **12**, 745–748.

Clayton R. N., Grossman L. and Mayeda T. K. (1973) A component of primitive nuclear composition in carbonaceous meteorites. *Science* **182**, 485–488.

Clayton R. N., Hinton R. W. and Davis A. M. (1988) Isotopic variations in the rock-forming elements in meteorites. *Phil. Trans. R. Soc. A* **325**, 483–501.

Clayton R. N. and Mayeda T. K. (1999) Oxygen isotope studies of carbonaceous chondrites. *Geochim. Cosmochim. Acta* **63**, 2089–2104.

Compston W. and Oversby V. M. (1969) Lead isotopic analysis using a double spike. *J. Geophys. Res.* **74**, 4338–4348.

Creech J. B. and Paul B. (2015) IsoSpike: improved double-spike inversion software. *Geostand. Geoanal. Res.* **39**, 7–15.

Day J. M. and Moynier F. (2014) Evaporative fractionation of volatile stable isotopes and their bearing on the origin of the Moon. *Phil. Trans. R. Soc. A* **372**. https://doi.org/10.1098/rsta.2013.0259.

Davis A. M. and Richter F. M. (2003) Condensation and evaporation of solar system materials. *Treatise Geochem.* **1**, 711. https://doi.org/10.1016/B0-08-043751-6/01067-7.

Davis A. M., Hashimoto A., Clayton R. N. and Mayeda T. K. (1990) Isotope mass fractionation during evaporation of Mg_2SiO_4. *Nature* **347**, 655–658.

Davis A. M., Zhang J., Greber N. D., Hu J., Tissot F. L. and Dauphas N. (2018) Titanium isotopes and rare earth patterns in CAIs: evidence for thermal processing and gas-dust decoupling in the protoplanetary disk. *Geochim. Cosmochim. Acta* **221**, 275–295.

de Laeter J. R., Böhlke J. K., De Bièvre P., Hidaka H., Peiser H. S., Rosman K. J. R. and Taylor P. D. P. (2003) Atomic weights of the elements. Review 2000 (IUPAC Technical Report). *Pure Appl. Chem.* **75**, 683–800.

De Maria G., Balducci G., Guido M. and Piacente V. (1971) Mass spectrometric investigation of the vaporization process of Apollo 12 lunar samples. *Lunar Planet. Sci. Conf. Proc.* **2**, 1367–1380.

Dodson M. H. (1969) A theoretical study of the use of internal standards for precise isotopic analysis by the surface ionization technique Part II: Error relationships. *J. Phys. E* **2**. https://doi.org/10.1088/0022-3735/2/6/306.

Eugster O., Tera F. and Wasserburg G. J. (1969) Isotopic analyses of barium in meteorites and in terrestrial samples. *J. Geophys. Res.* **74**, 3897–3908.

Fredriksson K. and Kerridge J. F. (1988) Carbonates and sulfates in CI chondrites: formation by aqueous activity on the parent body. *Meteorit. Planet. Sci.* **23**, 35–44.

Greber N. D., Dauphas N., Puchtel I. S., Hofmann B. A. and Arndt N. T. (2017a) Titanium stable isotopic variations in chondrites, achondrites and lunar rocks. *Geochim. Cosmochim. Acta* **213**, 534–552.

Greber N. D., Dauphas N., Bekker A., Ptáček M. P., Bindeman I. N. and Hofmann A. (2017b) Titanium isotopic evidence for felsic crust and plate tectonics 3.5 billion years ago. *Science* **357**, 1271–1274.

Hezel D. C. and Palme H. (2007) The conditions of chondrule formation, Part I: Closed system. *Geochim. Cosmochim. Acta* **71**, 4092–4107.

Hezel D. C. and Palme H. (2008) Constraints for chondrule formation from Ca–Al distribution in carbonaceous chondrites. *Earth Planet. Sci. Lett.* **265**, 716–725.

Hezel D. C. and Palme H. (2010) The chemical relationship between chondrules and matrix and the chondrule matrix complementarity. *Earth Planet. Sci. Lett.* **294**, 85–93.

Hin R. C., Coath C. D., Carter P. J., Nimmo F., Lai Y.-J., von Strandmann P. A. E. P., Willbold M., Leinhardt Z. M., Walter M. J. and Elliott T. (2017) Magnesium isotope evidence that accretional vapour loss shapes planetary compositions. *Nature* **549**, 511–515.

Huang S., Farkaš J. and Jacobsen S. B. (2010) Calcium isotopic fractionation between clinopyroxene and orthopyroxene from mantle peridotites. *Earth Planet. Sci. Lett.* **292**, 337–344.

Huang S. and Jacobsen S. B. (2017) Calcium isotopic compositions of chondrites. *Geochim. Cosmochim. Acta* **201**, 364–376.

Huang S., Farkaš J., Yu G., Petaev M. I. and Jacobsen S. B. (2012) Calcium isotopic ratios and rare earth element abundances in refractory inclusions from the Allende CV3 chondrite. *Geochim. Cosmochim. Acta* **77**, 252–265.

Jungck M. H. A., Shimamura T. and Lugmair (1984) Ca isotopic variations in Allende. *Geochim. Cosmochim. Acta* **48**, 2651–2658.

Kang J. T., Ionov D. A., Liu F., Zhang C. L., Golovin A. V., Qin L. P., Zhang Z. F. and Huang F. (2017) Calcium isotopic fractionation in mantle peridotites by melting and metasomatism and Ca isotope composition of the Bulk Silicate Earth. *Earth Planet. Sci. Lett.* **474**, 128–137.

Kato C. and Moynier F. (2017) Gallium isotopic evidence for extensive volatile loss from the Moon during its formation. *Sci. Adv.* **3**. https://doi.org/10.1126/sciadv.1700571.

Keil K. (1969) Titanium distribution in enstatite chondrites and achondrites, and its bearing on their origin. *Earth Planet. Sci. Lett.* **7**, 243–248.

Lodders K. (2003) Solar system abundances and condensation temperatures of the elements. *Astrophys. J.* **591**, 1220–1247.

Luck J. M., Othman D. B. and Albarède F. (2005) Zn and Cu isotopic variations in chondrites and iron meteorites: early solar nebula reservoirs and parent-body processes. *Geochim. Cosmochim. Acta* **69**, 5351–5363.

Mendybaev R. A., Richter F. M., Georg R. B., Janney P. E., Spicuzza M. J., Davis A. M. and Valley J. W. (2013) Experimental evaporation of Mg- and Si-rich melts: implications for the origin and evolution of FUN CAIs. *Geochim. Cosmochim. Acta* **123**, 368–384.

Millet M.-A. and Dauphas N. (2014) Ultra-precise titanium stable isotope measurements by double-spike high resolution MC-ICP-MS. *J. Anal. At. Spectrom.* **29**, 1444–1458.

Millet M.-A., Dauphas N., Greber N. D., Burton K. W., Dale C. W., Debret B., Macpherson C. G., Nowell G. M. and Williams H. M. (2016) Titanium stable isotope investigation of magmatic processes on the Earth and Moon. *Earth Planet. Sci. Lett.* **449**, 197–205.

Moynier F., Bouvier A., Blichert-Toft J., Telouk P., Gasperini D. and Albarède F. (2006) Europium isotopic variations in Allende CAIs and the nature of mass-dependent fractionation in the solar nebula. *Geochim. Cosmochim. Acta* **70**, 4287–4294.

Moynier F., Pringle E. A., Bouvier A. and Moureau J. (2015) Barium stable isotope composition of the Earth, meteorites, and calcium–aluminum-rich inclusions. *Chem. Geol.* **413**, 1–6.

Niederer F. R., Papanastassiou D. A. and Wasserburg G. J. (1985) Absolute isotopic abundances of Ti in meteorites. *Geochim. Cosmochim. Acta* **49**, 835–851.

Niederer F. R. and Papanastassiou D. A. (1984) Ca isotopes in refractory inclusions. *Geochim. Cosmochim. Acta* **48**, 1279–1293.

Niemeyer S. and Lugmair G. W. (1981) Ubiquitous isotopic anomalies in Ti from normal Allende inclusions. *Earth Planet. Sci. Lett.* **53**, 211–225.

Niemeyer S. and Lugmair G. W. (1984) Titanium isotopic anomalies in meteorites. *Geochim. Cosmochim. Acta* **48**, 2651–2658.

Paniello R. C., Day J. M. and Moynier F. (2012) Zinc isotopic evidence for the origin of the Moon. *Nature* **490**, 376–379.

Papanastassiou D. A. (1986) Chromium isotopic anomalies in the Allende meteorite. *Astrophys. J.* **308**, 27–30.

Pringle E. A., Moynier F., Savage P. S., Badro J. and Barrat J. A. (2014) Silicon isotopes in angrites and volatile loss in planetesimals. *Proc. Natl. Acad. Sci.* **111**, 17029–17032.

Pringle E. A. and Moynier F. (2017) Rubidium isotopic composition of the Earth, meteorites, and the Moon: evidence for the origin of volatile loss during planetary accretion. *Earth Planet. Sci. Lett.* **473**, 62–70.

Pringle E. A., Savage P. S., Jackson M. G., Barrat J. A. and Moynier F. (2013) Si isotope homogeneity of the solar nebula. *Astrophys. J.* **779**. https://doi.org/10.1088/0004-637X/779/2/123.

Richter F. M., Davis A. M., Ebel D. S. and Hashimoto A. (2002) Elemental and isotopic fractionation of Type B calcium-, aluminum-rich inclusions: Experiments, theoretical considerations, and constraints on their thermal evolution. *Geochimica. Cosmochimica. Acta* **66**, 521–540.

Richter F. M., Mendybaev R. A., Christensen J. N., Ebel D. and Gaffney A. (2011) Laboratory experiments bearing on the origin and evolution of olivine-rich chondrules. *Meteorit. Planet. Sci.* **46**, 1152–1178.

Rowe M. W., Clayton R. N. and Mayeda T. K. (1994) Oxygen isotopes in separated components of CI and CM meteorites. *Geochim. Cosmochim. Acta* **58**, 5341–5347.

Rudge J. F., Reynolds B. C. and Bourdon B. (2009) The double spike toolbox. *Chem. Geol.* **265**, 420–431.

Russell W. A., Papanastassiou D. A. and Tombrello T. A. (1978) Ca isotope fractionation on the Earth and other solar system materials. *Geochim. Cosmochim. Acta* **42**, 1075–1090.

Schiller M., Connelly J. N., Glad A. C., Mikouchi T. and Bizzarro M. (2015) Early accretion of protoplanets inferred from a reduced inner solar system ^{26}Al inventory. *Earth Planet. Sci. Lett.* **420**, 45–54.

Shahar A., Hillgren V. J., Young E. D., Fei Y., Macris C. A. and Deng L. (2011) High-temperature Si isotope fractionation between iron metal and silicate. *Geochim. Cosmochim. Acta* **75**, 7688–7697.

Simon J. I. and DePaolo D. J. (2010) Stable calcium isotopic composition of meteorites and rocky planets. *Earth Planet. Sci. Lett.* **289**, 457–466.

Simon J. I., DePaolo D. J. and Moynier F. (2009) Calcium isotope composition of meteorites, Earth, and Mars. *Astrophys. J.* **702**, 707–715.

Simon J. I., Jordan M. K., Tappa M. J., Schauble E. A., Kohl I. E. and Young E. D. (2017) Calcium and titanium isotope fractionation in refractory inclusions: tracers of condensation and inheritance in the early solar protoplanetary disk. *Earth Planet. Sci. Lett.* **472**, 277–288.

Sossi P. A., Nebel O. and Foden J. (2016) Iron isotope systematics in planetary reservoirs. *Earth Planet. Sci. Lett.* **452**, 295–308.

Sossi P. A., Moynier F., Chaussidon M., Villeneuve J., Kato C. and Gounelle M. (2017) Early solar system irradiation quantified by linked vanadium and beryllium isotope variations in meteorites. *Nat. Astron.* **1**. https://doi.org/10.1038/s41550-017-0055.

Sossi P. A. and O'Neill H. S. C. (2017) The effect of bonding environment on iron isotope fractionation between minerals at high temperature. *Geochim. Cosmochim. Acta* **196**, 121–143.

Steele R. C., Coath C. D., Regelous M., Russell S. and Elliott T. (2012) Neutron-poor nickel isotope anomalies in meteorites. *Astrophys. J.* **758**. https://doi.org/10.1088/0004-637X/758/1/59.

Teng F.-Z., Li W. Y., Ke S., Marty B., Dauphas N., Huang S., Wu F. Y. and Pourmand A. (2010) Magnesium isotopic composition of the Earth and chondrites. *Geochim. Cosmochim. Acta* **74**, 4150–4166.

Teng F.-Z., Watkins J. M. and Dauphas N. (2017) Non-traditional stable isotopes. *Rev. Mineral. Geochem.*, 82.

Trinquier A., Elliott T., Ulfbeck D., Coath C., Krot A. N. and Bizzarro M. (2009) Origin of nucleosynthetic isotope heterogeneity in the solar protoplanetary disk. *Science* **324**, 374–376.

Trinquier A., Birck J. L., Allègre C. J., Göpel C. and Ulfbeck D. (2008) ^{53}Mn–^{53}Cr systematics of the early Solar System revisited. *Geochim. Cosmochim. Acta* **72**, 5146–5163.

Valdes M. C., Moreira M., Foriel J. and Moynier F. (2014) The nature of Earth's building blocks as revealed by calcium isotopes. *Earth Planet. Sci. Lett.* **394**, 135–145.

Van Baalen M. R. (1993) Titanium mobility in metamorphic systems: a review. *Chem. Geol.* **110**, 233–249.

Weisberg M. K., Prinz M., Clayton R. N. and Mayeda T. K. (1993) The CR (Renazzo-type) carbonaceous chondrite group and its implications. *Geochim. Cosmochim. Acta* **57**, 1567–1586.

Williams, N.H., 2015. Titanium isotope cosmochemistry. Ph.D. thesis, Manchester University. (The PDF file of this thesis is available on the Manchester eScholar website: http://www.escholar.manchester.ac.uk/uk-ac-man-scw:259269).

Zhang J., Dauphas N., Davis A. M., Leya I. and Fedkin A. (2012) The proto-Earth as a significant source of lunar material. *Nat. Geosci.* **5**, 251–255.

Zhang J., Dauphas N., Davis A. M. and Pourmand A. (2011) A new method for MC-ICPMS measurement of titanium isotopic composition: identification of correlated isotope anomalies in meteorites. *J. Anal. At. Spectrom.* **26**, 2197–2205.

Zhang J., Huang S., Davis A. M., Dauphas N., Hashimoto A. and Jacobsen S. B. (2014) Calcium and titanium isotopic fractionations during evaporation. *Geochim. Cosmochim. Acta* **140**, 365–380.

Associate editor: Dimitri A. Papanastassiou